

# Interaction Pattern Disentangling for Multi-Agent Reinforcement Learning

Shunyu Liu, Jie Song, Yihe Zhou, Na Yu, Kaixuan Chen, Zunlei Feng, Mingli Song

**Abstract**—Deep cooperative multi-agent reinforcement learning has demonstrated its remarkable success over a wide spectrum of complex control tasks. However, recent advances in multi-agent learning mainly focus on value decomposition while leaving entity interactions still intertwined, which easily leads to over-fitting on noisy interactions between entities. In this work, we introduce a novel *interactiOn Pattern disenTangling* (OPT) method, to disentangle not only the joint value function into agent-wise value functions for decentralized execution, but also the entity interactions into interaction prototypes, each of which represents an underlying interaction pattern within a sub-group of the entities. OPT facilitates filtering the noisy interactions between irrelevant entities and thus significantly improves generalizability as well as interpretability. Specifically, OPT introduces a sparse disagreement mechanism to encourage sparsity and diversity among discovered interaction prototypes. Then the model selectively restructures these prototypes into a compact interaction pattern by an aggregator with learnable weights. To alleviate the training instability issue caused by partial observability, we propose to maximize the mutual information between the aggregation weights and the history behaviors of each agent. Experiments on both single-task and multi-task benchmarks demonstrate that the proposed method yields results superior to the state-of-the-art counterparts. Our code will be made publicly available.

**Index Terms**—Deep Reinforcement Learning, Cooperative Multi-Agent Learning, Interaction Pattern Disentangling.

## 1 INTRODUCTION

REINFORCEMENT learning (RL) is instigated by the *trial and error* (TE) procedure in human behaviors and now becomes a well-established paradigm for building intelligent systems interacting with the environment, especially driven by the resurgence of deep learning [1], [2], [3]. In the RL context, cooperative multi-agent reinforcement learning (MARL), where a group of agents works collaboratively for one common goal, is a long-standing research topic and a key tool used to address many real-world problems such as video games [4], [5], traffic light systems [6], and smart grid control [7], [8], [9]. However, cooperative MARL is perceived as a significantly more challenging problem than the single-agent counterpart due to several peculiar characteristics, for example, *credit assignment* that the agents need to deduce their contributions in the presence of only global rewards, *partial observability* which necessitates the learning of decentralized policies, the *curse of dimensionality* that the joint action (and state) space grows exponentially with the number of agents, *etc.*

To alleviate these issues, value-based MARL has recently emerged as a powerful framework with the large capacity of deep neural networks and the *centralized training and decentralized execution* (CTDE) paradigm [10], [11], [12], [13]. Value-based MARL endows agents the ability to learn the individual optimal policies by decomposing the global value function according to their contributions. For

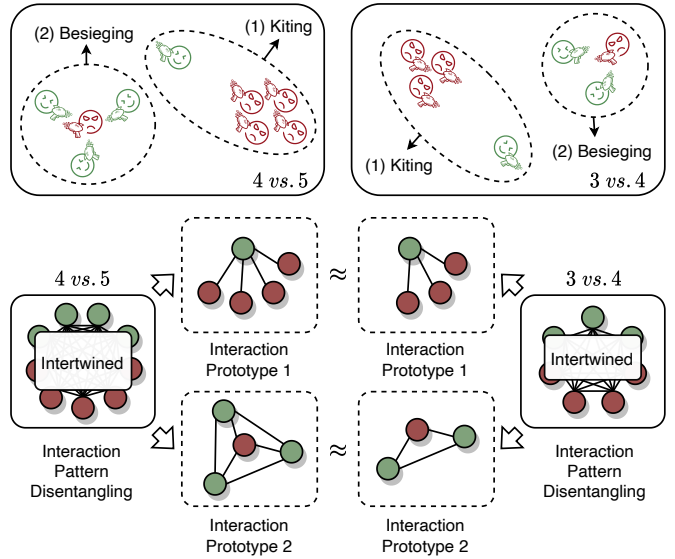


Fig. 1: A visualization example of two shooting tasks with different scales. Green and red indicate the agents and enemies, respectively. The intertwined interaction patterns is disentangled into two interaction prototypes: (1) One agent kites most of the enemies. (2) The other agents besiege the alone enemy.

- S. Liu, Y. Zhou, N. Yu, K. Chen, and M. Song are with the College of Computer Science and Technology, Zhejiang University, Hangzhou 310027, China. E-mail: liushunyu@zju.edu.cn, yihe\_zhou@zju.edu.cn, na\_yu@zju.edu.cn, chenx@zju.edu.cn, brooksong@zju.edu.cn.
- J. Song, Z. Feng are with the College of Software Technology, Zhejiang University, Hangzhou 310027, China. E-mail: sjie@zju.edu.cn, zunleifeng@zju.edu.cn.

(Corresponding author: Jie Song.)

example, value decomposition network (VDN) [10] learns to additively factorize the team value function into agent-wise value functions, which enables the decentralized deployment of the centralized trained agents. QMIX [11] identifies that the full factorization of VDN is not necessary and employs a network that estimates joint action values as a complex non-linear combination of per-agent values that condi-

tion only on local observations. Furthermore, randomized entity-wise factorization for imagined learning (REFIL) [13] randomly divided entities into sub-groups to construct an auxiliary regularization term, which facilitates discovering more generalized value functions. These works mainly focus on agent-wise value decomposition with centralized training for decentralized deployment. The decentralized policies, however, can generalize poorly at test time due to over-fitting on noisy interaction patterns during the training time. Specifically, as depicted in Figure 1, different interaction patterns often simultaneously exist among entities in a complex environment. The interaction patterns concealed in various-scale tasks are usually shareable, resulting in similar sub-group strategies of agents. However, these patterns are closely intertwined and denoted merely as a single dense attention distribution between the entities in the existing methods [12], [13], [14], [15]. Each agent is trained to pay attention to all observable entities, including the irrelevant ones. These irrelevant entities can be considered as noisy information, severely impeding the extraction of interaction patterns and downgrading the model generalizability.

In this work, we thus propose *interaction Pattern disentangling*, abbreviated as OPT, to explicitly conduct interaction pattern disentangling for MARL. Unlike prior methods devoted to value decomposition while leaving latent interaction patterns entangled between entities, the proposed OPT disentangles not only the joint value function into agent-wise value functions for decentralized execution, but also the entity interactions into several *interaction prototypes*. Each prototype in the proposed method represents an underlying interaction pattern within a sub-group of the entities, which facilitates filtering the noisy interactions between irrelevant entities and thus improves the generalizability and interpretability. Technically, we adopt a sparse activation function with a contrastive disagreement objective function to extract both sparse and diverse interaction prototypes. To derive the final policy, we selectively recombine these prototypes by an aggregator with learnable weights, unweighting the irrelevant prototypes and emphasizing the important ones. Moreover, we propose to maximize the mutual information between the aggregation weights and the history behaviors to alleviate the training instability issue caused by the partial observability. To sum up, we make the following contributions in this work:

- We identify the entangled interaction problem in MARL, and introduce the interaction pattern disentangling task for cooperative MARL, a highly important ingredient for generalization yet largely overlooked by existing literature.
- We propose OPT, a novel disentangling method to decompose entity interactions into interaction prototypes. OPT not only enjoys stronger generalizability, but also exhibits higher interpretability with the disentangled interaction prototypes.
- Experiments conducted on several StarCraft II micromanagement benchmarks demonstrate that OPT yields significantly superior performance to state-of-the-art competitors in both single-task and multi-task MARL settings.

The remainder of this manuscript is organized as fol-

lows. In Section 2, we briefly review some topics highly related to this work, including value decomposition and interaction pattern in MARL. Then preliminaries of MARL are provided in Section 3. The proposed interaction pattern disentangling is provided in Section 4. Experimental results, including the benchmark comparison and ablation study, are presented in Section 5. Finally, we conclude this manuscript with some possible future works in Section 6.

## 2 RELATED WORK

We briefly review here some topics that are most related to the proposed work, including value decomposition and interaction pattern in MARL.

### 2.1 Value Decomposition in MARL

Deep cooperative MARL has been an active research topic in recent years [16], [17], [18], [19], [20], [21]. The most common approach to this problem heretofore is to learn value decomposition under the CTDE paradigm. To enable effective CTDE, the Individual-Global-Max (IGM) principle guarantees the optimal consistency between the joint and individual actions [22]. Based on this IGM principle, VDN [10] factorizes the joint action-value function into a summation of individual agent terms. In contrast, QMIX [11] extends this additive value function factorization and imposes a monotonicity constraint. Furthermore, QTRAN [22], WQMIX [23], and QPLEX [12] progressively enlarged the family of functions that the mixing network can represent. QTRAN [22] introduces the regularization constraints to avoid the representation limitations of VDN and QMIX. WQMIX [23] improves QMIX by a weighted projection that places more emphasis on better joint actions. QPLEX [12] proposes a duplex dueling network architecture to factorize the value function and has shown state-of-the-art performance on challenging tasks. In addition, other advanced works exploit the value decomposition from the perspective of role-based learning [24], [25], large-scale transfer learning [26], [27], [28], and intrinsic motivation-driven exploration [29], [30], [31], [32], [33]. However, these works still treat all entities as a whole and ignore their internal interaction information.

### 2.2 Interaction Pattern in MARL

Exploring complex interaction patterns has been widely studied in MARL. DGN [34] models the multi-agent environment as a graph structure, where the graph convolutional network captures the interplay between agents by their latent representations. Moreover, NCC [35] assumed that the agents could achieve better cooperation if all neighboring agents formed consistent neighborhood cognition based on the predefined graph. To further utilize sub-group relationships, HAMA [36] divides all the entities into distinct sub-graphs using prior rules before learning. However, the prior relationships between entities are often unavailable. On the other hand, MAAC [14] introduces the attention mechanism to learn the interaction relationships, while ATOC [15] exploits attentional communication to make cooperative decisions. UPDeT [37] and PIT [38] utilize

attention-based semantic alignment between the input entities and the output actions to decompose the policy. Despite the promising results achieved, these works mainly rely on dense attention and have to focus on the irrelevance entities.

To remedy this issue, ALC-MADDPG [39] and CASEC [40] use the predefined threshold to prune the low correlation relationships between agents, while G2ANet [41] and S2RL [42] introduce the sparse attention mechanism to learn the dynamics among agents. Furthermore, REFIL [13] randomly partitions entities into sparse sub-groups and forces each sub-group to learn the same objective function as all entities. This random grouping strategy serves as a regularization term to improve the generalization ability of value functions. Nevertheless, the interaction patterns in these methods still remain entangled. They only consider the sparsity of interaction patterns but ignore the diversity. Different interaction patterns often simultaneously exist among entities in a complex task. To this end, we introduce a novel method to realize the interaction pattern disentangling for both sparsity and diversity.

### 3 PRELIMINARY

In this section, we formally define the cooperative MARL problem under the *decentralized partially observable Markov decision process* (Dec-POMDP) with entities. Then we introduce the *centralized training and decentralized execution* (CTDE) paradigm for value decomposition.

#### 3.1 Dec-POMDP with Entities

Cooperative MARL problem can be described as a Dec-POMDP with entities [13], [43] defined by a tuple  $\langle \mathcal{E}, \mathcal{A}, \mathcal{T}, \mathcal{S}, \mathcal{U}, P, r, \Omega, O, \gamma \rangle$ , where  $\mathcal{E}$  is the set of entities in the environment. Each entity  $e$  has a state representation  $s^e$  and  $s = \{s^e \mid e \in \mathcal{E}\} \in \mathcal{S}$  is the global state of the environment.  $\mathcal{A} \subseteq \mathcal{E}$  is the finite set of agents, while the non-agent entities are part of the environment (e.g. uncontrollable enemies, obstacles and landmarks).  $\mathcal{T}$  is the set of tasks, where each task is composed of different number of entities and agents. At each time step  $t$ , each agent  $a \in \mathcal{A}$  receives an individual partial observation  $o_t^a \in \Omega$  according to the observation function  $O(s_t, a)$  and chooses an action  $u_t^a \in \mathcal{U}$ , forming a joint action  $\mathbf{u}_t$ . This causes a transition to the next state  $s_{t+1}$  according to the state transition function  $P(s_{t+1} \mid s_t, \mathbf{u}_t)$ . All agents share the same reward function  $r(s_t, \mathbf{u}_t)$  and  $\gamma \in [0, 1)$  is the discount factor. Each agent  $i$  has an action-observation history  $\tau^a \in \mathcal{T} \equiv (\Omega \times \mathcal{U})^*$  and learns its individual policy  $\pi^a(u^a | \tau^a)$  to jointly maximize the discounted return  $R_t = \sum_{k=0}^{\infty} \gamma^k r_{t+k}$ .  $\tau$  is used to denote joint action-observation history. The joint policy  $\pi$  induces a joint action-value function  $Q_{tot}^{\pi}(s_t, \mathbf{u}_t) = \mathbb{E}_{s_{t+1:\infty}, \mathbf{u}_{t+1:\infty}} [R_t \mid s_t, \mathbf{u}_t]$ .

#### 3.2 CTDE Paradigm

The CTDE paradigm allows agents to learn their individual utility functions by optimizing the joint action-value function for credit assignment, which has been widely used in deep multi-agent reinforcement learning [44], [45], [46], [47]. During centralized training, the learning model has

access to the global state and the action-observation histories of all agents, whereas each agent can only condition on its own action-observation history during decentralized execution. Due to the partial observability,  $Q_{tot}(\tau, \mathbf{u}, s)$  is used in place of  $Q_{tot}(\mathbf{u}, s)$ . A mixing network is introduced to merge all individual action values into a joint one  $Q_{tot}(\tau, \mathbf{u}, s; \theta_v) = f([Q_a(\tau^a, u^a; \theta_\pi)]_a, s; \theta_v)$ , where  $Q_a$  is the utility network of each agent  $a$ . The learnable parameter  $\theta = \{\theta_\pi, \theta_v\}$  can be updated by minimizing the following expected Temporal-Difference (TD) loss:

$$\mathcal{L}_{TD}(\theta) = \mathbb{E}_{\mathcal{D}} \left[ (y^{tot} - Q_{tot}(\tau, \mathbf{u}, s; \theta_v))^2 \right]. \quad (1)$$

where  $\mathcal{D}$  is the replay buffer of the transitions,  $y^{tot} = r + \gamma \max_{\mathbf{u}'} Q_{tot}(\tau', \mathbf{u}', s'; \theta_v^-)$  and  $\theta_v^-$  is the parameter of the target network [2].

### 4 METHOD

In what follows, we first provide an overview of the framework based on the proposed *interactiOn Pattern disenTangling* (OPT) module, as shown in Figure 2. Our framework adopts the CTDE paradigm, where each agent learns its individual utility network by optimizing the TD loss of the mixing network. We further detail our OPT method, as shown in Figure 3. We start by introducing the explicit disentangling step, which is based on a sparse disagreement mechanism. Then we describe the restructuring process with a temporal-stable aggregator and finally summarize the complete optimization objective.

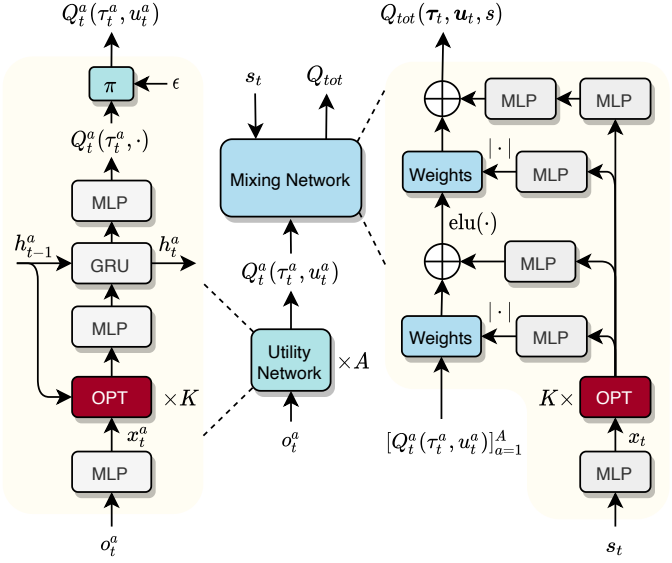


Fig. 2: An overview of the framework based on the proposed *interactiOn Pattern disenTangling* (OPT) method. The middle is the basic MARL framework under the CTDE paradigm, where we use the OPT module in both the utility network and mixing network. The left is the utility network of each agent, and the right is the mixing network.

#### 4.1 Overall Framework

As shown in Figure 2, the OPT serves as a plug-in module in both the utility network and mixing network under the

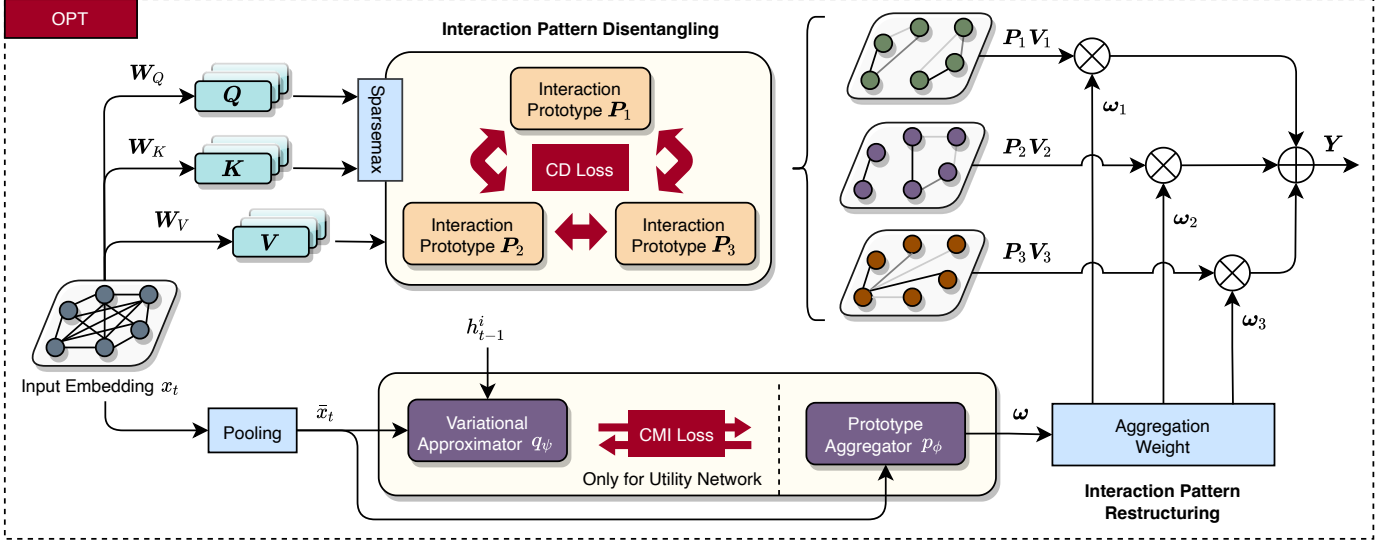


Fig. 3: An illustrative diagram of the proposed *interaction Pattern disentangling* (OPT) method, which mainly consists of two steps: disentangling and restructuring.

CTDE paradigm, jointly facilitating the learning of decision making and credit assignment. We use a transformer architecture [48] to stack multiple layers of OPT modules, which can promote the generalization ability of the model. The outputs of the OPT modules are directly used for subsequent network computations. All the network modules, including OPT, MLP and GRU, perform entity-wise operations on their input.

Specially, the utility network of each agent  $a$  takes the current observation  $o_t^a$  and the history information  $h_{t-1}^a$  as input, estimating the individual action value  $Q_t^a(\tau_t^a, \cdot)$  based on the OPT module. Moreover, each action value is calculated by its corresponding entity. Then the agent  $a$  selects an action  $u_t^a$  that maximizes the action value  $Q_t^a(\tau_t^a, \cdot)$  to execute in the environment, while the action value  $Q_t^a(\tau_t^a, u_t^a)$  is used as the input to the mixing network. Here we adopt the annealed  $\epsilon$ -greedy strategy for exploration. Our mixing network implementation uses QMIX [11] as a basic backbone for its robust performance, but it is readily applicable to the other mixing method. The mixing network is a feed-forward neural network that merge all individual action values into a joint one  $Q_{tot}(\tau, u, s; \theta_v)$ , where the weights of the mixing network are generated by a hyper-network that takes the global state  $s_t$  as input. The OPT module is used to handle the global state  $s_t$  in this hyper-network of the mixing network.

## 4.2 Disentangling

The goal of disentangling step is to explore the diverse interaction prototypes from the input observation or state of entities. The method we adapt to generate these prototypes is based on the self-attention module in transformer, which can capture the relationship weights between each pair of entities. The disentangling steps of the utility network and mixing network are similar except for different inputs. Thus, we use the mixing network as an example to describe this process.

At each time step  $t$ , the input state of the mixing network is defined as  $s_t = [s_t^1, \dots, s_t^M]^T \in \mathbb{R}^{M \times d_e}$ , where  $M$  is the number of the entities and  $d_e$  is the state representation dimension of the entity. We first encode the state representation of each entity  $s_t^e$  via an entity-wise embedding function  $f(\cdot) : \mathbb{R}^{d_e} \rightarrow \mathbb{R}^{d_x}$  and output the embedding feature  $x_t^e = f(s_t^e)$  with the dimension of  $d_x$ . Then the input of the disentangling step is denoted as  $x_t = [x_t^1, \dots, x_t^M]^T \in \mathbb{R}^{M \times d_x}$ . We assume that entities treat each other equally before disentangling, forming a fully connected interaction pattern. Therefore, our method focuses on disentangling this fully connected pattern into several interaction prototypes.

Each interaction prototype can be described as an attention map where the relationship weights between entities are computed by the query with the corresponding key. To simplify the following description, the embedding matrix  $\mathbf{X}$  is used instead of  $x_t$ . Specifically, we first transform the input embedding  $\mathbf{X}$  into queries  $\mathbf{Q} \in \mathbb{R}^{M \times d_x}$ , keys  $\mathbf{K} \in \mathbb{R}^{M \times d_x}$ , and values  $\mathbf{V} \in \mathbb{R}^{M \times d_x}$ :

$$\begin{bmatrix} \mathbf{Q} \\ \mathbf{K} \\ \mathbf{V} \end{bmatrix} = \mathbf{X} \begin{bmatrix} \mathbf{W}_Q \\ \mathbf{W}_K \\ \mathbf{W}_V \end{bmatrix}, \quad (2)$$

where  $\varphi = \{\mathbf{W}_Q, \mathbf{W}_K, \mathbf{W}_V\}$  are parameter matrices and each matrix  $\mathbf{W} \in \mathbb{R}^{d_x \times d_x}$  is trainable. Then we can calculate the dot product for queries and keys to obtain the relationship weights between entities, followed by an activation function to normalize the output weights to a probability distribution.

The conventional activation function used for normalization is the softmax function, which never assigns a probability of zero to any weights. Due to the strictly positive probabilities, we can never rule out the irrelevant entities for the interaction prototypes. This density is wasteful and noisy, making the exploration space more complex. In a particular interaction prototype, an entity usually interacts with only several crucial entities, which implies a sparsity constraint over the probability distribution. Thus, a sparse

activation function is desired to focus on the importance entities and ignore the irrelevant entities. Inspired by the sparse mechanism used in [49], [50], we introduce sparsemax as an alternative to softmax, which tends to yield sparse probability distribution:

$$\text{sparsemax}(\mathbf{z}) := \arg \min_{\mathbf{p} \in \Delta^M} \|\mathbf{p} - \mathbf{z}\|_2, \quad (3)$$

where  $\mathbf{z} \in \mathbb{R}^M$  is the input vector and  $\mathbf{p} \in \mathbb{R}^M$  is the output vector.  $\Delta^M := \{\mathbf{p} \in \mathbb{R}^M \mid \mathbf{p} \geq 0, \|\mathbf{p}\|_1 = 1\}$  is the probability simplex. Sparsemax realizes a Euclidean projection of the input vector onto the probability simplex, which is likely to hit the boundary of the simplex and obtain the sparse solution. The solution of Eq. 3 is obtained as follows:

$$\mathbf{p} = [\mathbf{z} - \sigma(\mathbf{z})\mathbf{1}]_+, \quad (4)$$

where  $[\cdot]_+ = \max(0, \cdot)$  is a clipping function and  $\mathbf{1} \in \mathbb{R}^M$  denotes the all-one vector.  $\sigma(\cdot) : \mathbb{R}^M \rightarrow \mathbb{R}$  is a threshold function. We first sort the elements of vector  $\mathbf{z}$  in descending order to derive a sorted vector  $\hat{\mathbf{z}}$ . Then the number of non-zero elements in the sparse solution  $\mathbf{p}$  is calculated as

$$m(\hat{\mathbf{z}}) = \arg \max_{m \in \{1, 2, \dots, M\}} \left\{ m\hat{z}_m > \sum_{i \leq m} \hat{z}_i - 1 \right\}. \quad (5)$$

Thus, the threshold value is given by

$$\sigma(\mathbf{z}) = \frac{\left( \sum_{i \leq m(\hat{\mathbf{z}})} \hat{z}_i - 1 \right)}{m(\hat{\mathbf{z}})}. \quad (6)$$

It is easy to prove that  $\sigma(\mathbf{z})$  satisfies  $\sum_i [\mathbf{z}_i - \sigma(\mathbf{z})]_+ = 1$  for every  $\mathbf{z}$ . In this way, we can directly calculate the sparse probability distribution based on the threshold value. Sparsemax can retain most of the important properties of softmax, and meanwhile assign exactly zero probability to low-scoring choices.

This sparsity enables us to discover similar sub-group entities and promotes the generalization of the generated interaction prototypes. Consequently, an interaction prototype is constructed by

$$\mathbf{P} = \text{sparsemax} \left( \frac{\mathbf{Q}\mathbf{K}^T}{\sqrt{d_x}} \right), \quad (7)$$

where  $\sqrt{d_x}$  is the scaling coefficient. We construct  $N$  interaction prototypes. Each prototype can be represented by  $\mathbf{P}_n \in \mathbb{R}^{M \times M}$  with its own trainable parameter matrices  $\varphi_n$ . Moreover, the corresponding value matrix is defined as  $\mathbf{V}_n$ . Then these prototypes will be used for the next restructuring step. However, without any other constraint, some generated interaction prototypes may contain a similar structure, degrading the disentanglement performance and capacity of the model. We therefore design an additional loss function in the disentangle step, aiming to avoid the similarity of the generated interaction prototypes.

The motivation of the additional loss function is that, a well disentangled interaction prototype should be clearly distinguished from the others. However, obtaining the solution that all the disentangled interaction prototypes differ from each other without any constraint will severely damage the performance. The distance between different prototypes can be infinitely enlarged, resulting in divergence of

the optimization process. We thus constrain the solution by using a contrastive disagreement (CD) loss:

$$\mathcal{L}_{CD}(\theta, \varphi) = \mathbb{E}_{n,e} \left[ -\log \left( \frac{\exp \left( (\mathbf{P}_n^e \mathbf{V}_n)^T \mathbf{P}_n^e \mathbf{V}_n \right)}{\sum_{i=1}^N \exp \left( (\mathbf{P}_n^e \mathbf{V}_n)^T \mathbf{P}_i^e \mathbf{V}_i \right)} \right) \right], \quad (8)$$

where  $\mathbf{P}_n^e \in \mathbb{R}^{1 \times M}$  is the interaction prototype of the entity  $e$ . In the contrastive disagreement loss, we use the prototype itself as the positive sample and the other prototypes as the negative sample. In this way, this loss only focuses on the negative prototypes and constrains them to uniformly distribute on a hypersphere without divergence [51]. With the contrastive disagreement loss, we directly encourage the diversity among interaction prototypes. This diversity enables the model to provide discriminative interaction prototypes for different tasks.

### 4.3 Restructuring

In the restructuring step, we aim to selectively restructure the interaction prototypes to form the final compact pattern. The input embedding  $x_t \in \mathbb{R}^{M \times d_x}$  of the restructuring step is the same as the previous disentangling step. Firstly, we use a mean pooling operation to extract the global information  $\bar{x}_t \in \mathbb{R}^{d_x}$  from  $x_t$  over all entities. Then the prototype aggregator  $p_\phi : \mathbb{R}^{d_x} \rightarrow \mathbb{R}^N$  takes  $\bar{x}_t$  as input to derive the aggregation weights  $\omega \in \mathbb{R}^N$ . The prototype aggregator  $p_\phi$  parameterized by  $\phi$  is a one-layer mlp network with softmax function. Then we use the aggregation weights  $\omega$  to restructure the interaction prototypes and output the final compact pattern  $\mathbf{Y} = \sum_{n=1}^N \omega_n \mathbf{P}_n \mathbf{V}_n \in \mathbb{R}^{M \times d_x}$ . The restructuring processing could facilitate the extraction of global information while adapting to different interaction prototypes with learnable weights. Then the output pattern is employed for the following decision making in the utility network or credit assignment in the mixing network.

Although the global state could be computed directly in the mixing network, the observation information in the utility network is incomplete due to the partial observability, resulting in the instability of the aggregation weights. To prevent this, we propose a conditional mutual information (CMI) objective:

$$I(\omega^a; \tau_{t-1}^a | o_t^a) = H(\omega^a | o_t^a) - H(\omega^a | \tau_{t-1}^a, o_t^a) \quad (9)$$

where  $H$  is the entropy and the aggregator of the agent  $a$  are regularized not only conditioned on its observation but also its history behaviors. Therefore, we can stabilize the generated aggregation weights over time via maximizing the CMI objective. However, directly optimizing this objective is quite difficult, so we design a variational approximator  $q_\psi$  parameterised by  $\psi$  to approximate the posterior over  $\omega_t^a$  given the observed trajectories [24], [29]. The variational inference provides a lower bound of the CMI objective to optimize, which can be formalized as a loss function:

$$\mathcal{L}_{CMI}(\theta, \phi, \psi) = \mathbb{E}_{\mathcal{D}} \left[ \text{KL} [p_\phi(\omega_t^a | \bar{x}_t^a) \parallel q_\psi(\omega_t^a | h_{t-1}^a, \bar{x}_t^a)] \right], \quad (10)$$

where  $\text{KL}(\cdot)$  is the KL divergence function,  $\bar{x}_t^a$  is the input embedding of the observation  $o_t^a$  after mean pooling operation, and a GRU network [52] is used to encode the history

trajectory  $\tau_{t-1}^a$  into  $h_{t-1}^a$ . Compared to directly relying the aggregator on history behaviors, the CMI objective derives a tractable lower bound, which provides a more solid objective to optimize. The proof is given in the appendix.

#### 4.4 Optimization Objective

To sum up, training our framework based on the OPT module contains three main parts. The first one is the original TD loss  $\mathcal{L}_{TD}$ , which enables each agent to learn its individual policy by optimizing the joint action value of the mixing network. The second one is the CD loss  $\mathcal{L}_{CD}$  to facilitate the sparsity and diversity among interaction prototypes when disentangling. The last one is the CMI loss  $\mathcal{L}_{CMI}$  to stabilize the aggregation weights for restructuring. Thus, given the three corresponding loss items, the total loss of our framework is formulated as follows:

$$\mathcal{L}(\theta, \varphi, \phi, \psi) = \mathcal{L}_{TD}(\theta) + \alpha \mathcal{L}_{CD}(\theta, \varphi) + \beta \mathcal{L}_{CMI}(\theta, \phi, \psi), \quad (11)$$

where the  $\alpha$  and  $\beta$  are coefficients. The overall framework is trained in an end-to-end centralized manner. We summarize the full procedure in Algorithm 1.

---

#### Algorithm 1 OPT for Multi-Agent Reinforcement Learning

**Initialize:** Utility network  $\theta_\pi$ , mixing network  $\theta_v$ , target network  $\theta_v^- = \theta_v$ , replay buffer  $\mathcal{D}$

```

1: repeat
2:   ▷ Collect the data
3:   Sample a task from  $\mathcal{T}$ 
4:   Obtain the initial global state  $s_0$ 
5:   while not terminal do
6:     for each agent  $a$  do:
7:       Obtain the observation  $o_t^a = O(s_t, a)$ 
8:       Calculate the input embedding  $x_t^a$ 
9:       ▷ Disentangling
10:      Calculate  $\{\mathbf{Q}_{t,n}^a, \mathbf{K}_{t,n}^a, \mathbf{V}_{t,n}^a\}_{n=1}^N$ 
11:      Extract the interaction prototypes  $\{\mathbf{P}_{t,n}^a\}_{n=1}^N$ 
12:      ▷ Restructuring
13:      Calculate the aggregation weights  $\omega_t^a$ 
14:      Construct the final compact patterns  $\mathbf{Y}_{t,n}^a$ 
15:      ▷ Policy
16:      Calculate  $h_t^a = \text{GRU}(\mathbf{Y}_{t,n}^a, h_{t-1}^a)$ 
17:      Calculate the action values  $Q_t^a(h_t^a, \cdot)$ 
18:      Sample  $u_t^a$  from  $Q_t^a(h_t^a, \cdot)$  based on  $\epsilon$ -greedy
19:    end for
20:    Execute the joint action  $\mathbf{u}_t = [u_t^1, \dots, u_t^K]$ 
21:    Receive the reward  $r_{t+1}$  and the next state  $s_{t+1}$ 
22:  end while
23:  Store the episode to the replay buffer  $\mathcal{D}$ 
24:  ▷ Train the networks
25:  Sample episodes from the replay buffer  $\mathcal{D}$ 
26:  Calculate joint action values with mixing network
27:  Compute  $\mathcal{L}_{TD}(\theta), \mathcal{L}_{CD}(\theta, \varphi), \mathcal{L}_{CMI}(\theta, \phi, \psi)$ 
28:  Update the network parameters  $\theta, \varphi, \phi, \psi$ 
29:  Update the target network  $\theta_v^- = \theta_v$  every  $C$  episodes
30: until converge

```

---

## 5 EXPERIMENTS

To demonstrate the effectiveness of the proposed interaction pattern disentangling (OPT) method, experiments are conducted based on the complex StarCraft Multi-Agent Challenge (SMAC)<sup>1</sup> [53], which has become a common-used benchmark for evaluating state-of-the-art MARL approaches. SMAC focuses on micromanagement challenges where each of the ally entities is controlled by an individual learning agent, and enemy entities are controlled by a built-in AI. The goal of the agents is to maximize the damage to enemies. Hence proper tactics such as focusing fire and avoiding overkill are required during battles. Learning these diverse interaction behaviors under partial observation is a challenging task.

Our methods are compared with various state-of-the-art baseline methods in both single-task [53] and multi-task [13] settings. We adopt the Python MARL framework (PyMARL) [53] to run all experiments. The hyperparameters of the baselines are the same as those in PyMARL and referred in their source codes. The implementation of our method is also based on PyMARL. The detailed hyperparameters are given as follows, where the common training parameters across different baselines are consistent to ensure comparability. For the OPT module in all experiments, we set the layer number  $K$  to 2, the interaction prototype number  $N$  to 4, and the interaction prototype dimension  $d_x$  to 32. The CD loss coefficient  $\alpha$  is set to 0.5, and the CMI loss coefficient  $\beta$  is set to 0.1. Batches of 32 episodes are sampled from the replay buffer with the size of 5K every training iteration. The target update interval is set to 200, and the discount factor is set to 0.99. We use the RMSprop Optimizer with a learning rate of  $5 \times 10^{-4}$ , a smoothing constant of 0.99, and with no momentum or weight decay. For exploration,  $\epsilon$ -greedy is used with  $\epsilon$  annealed linearly from 1.0 to 0.05 over 50K training steps and kept constant for the rest of the training. We modify several hyperparameters in some difficult scenarios and detail them below. In the following, we will first introduce the environments and the baselines, and then the results of different methods and ablations.

### 5.1 Single-task Environment

To validate the effectiveness of our methods in single-task setting, we conduct experiments on 6 single-task SMAC scenarios [53] which are classified into **Easy** (*10m\_vs\_11m*), **Hard** (*5m\_vs\_6m*) and **Super Hard** (*MMM2*, *corridor*, *6h\_vs\_8z*, *3s5z\_vs\_3s6z*). Two of these scenarios are homogeneous (*10m\_vs\_11m*, *5m\_vs\_6m*), where the army is composed of only a single unit type, while the others are heterogeneous. We compare the proposed OPT with various MARL baselines: IQL [53], VDN [10], QMIX [11], QTRAN [22], QPLEX [12], OWQMIX and CWQMIX [23]. For the super hard scenarios that require more exploration, the test win rates often remain 0% with the default hyperparameters. In this way, we extend the epsilon anneal time to 500K, and two of them (*corridor*, *6h\_vs\_8z*) optimized with the Adam Optimizer for all the compared methods.

The experimental results on different single-task scenarios are shown in Figure 4 and Table 1. Compared with

1. We use SC2.4.10 version instead of the older SC2.4.6.2.69232. Performance is not comparable across versions.

the state-of-the-art baseline methods in both easy and hard homogeneous scenarios (*10m\_vs\_11m*, *5m\_vs\_6m*), our proposed OPT successfully improves the learning efficiency and the final performance. In the easy homogeneous scenario (*10m\_vs\_11m*), the size of the armed forces between the agents and enemies is similar. Thus, several baselines,

including VDN and QMIX, can also achieve the promising results with additive or monotonic value factorization, while the exploratory benefit brought by interaction pattern disentangling is not obvious. However, in the more difficult homogeneous scenario (*5m\_vs\_6m*), our method consistently outperforms baselines by a large margin during

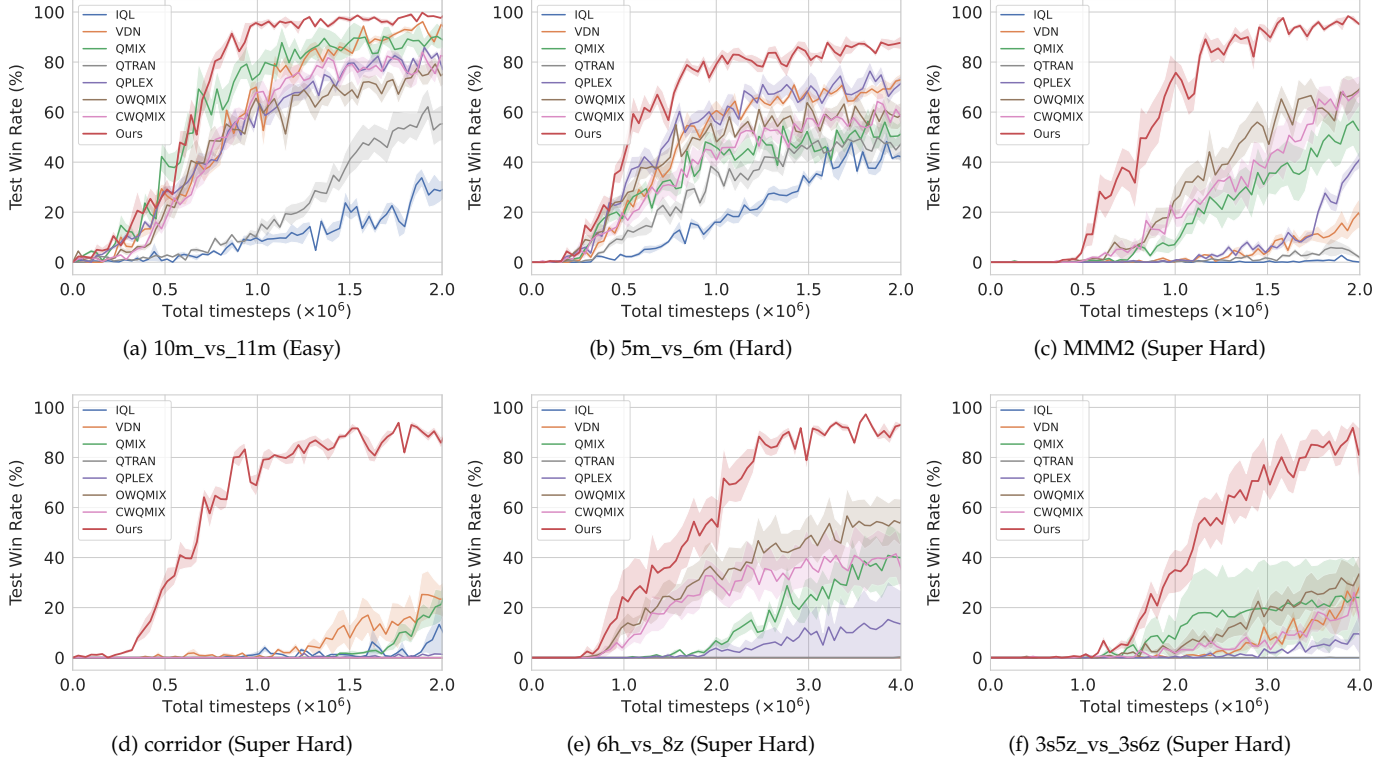


Fig. 4: Learning curves of our method and baselines in 6 single-task SMAC scenarios. All experimental results are illustrated with the median performance and 25-75% percentiles (shaded region) over 5 random seeds for a fair comparison.

TABLE 1: The area under curve and test win rate of our method and baselines in 6 single-task SMAC scenarios.  $\pm$  corresponds to one standard deviation of the average evaluation over 5 trials. **Bold** indicates the best performance in each SMAC scenario.

	Method	10m_vs_11m	5m_vs_6m	MMM2	corridor	6h_vs_8z	3s5z_vs_3s6z
Area Under Curve	IQL [53]	$0.09 \pm 0.04$	$0.19 \pm 0.03$	$0.00 \pm 0.00$	$0.01 \pm 0.01$	$0.00 \pm 0.00$	$0.00 \pm 0.00$
	VDN [10]	$0.55 \pm 0.02$	$0.44 \pm 0.04$	$0.03 \pm 0.03$	$0.05 \pm 0.06$	$0.00 \pm 0.00$	$0.05 \pm 0.04$
	QMIX [11]	$0.61 \pm 0.12$	$0.33 \pm 0.10$	$0.17 \pm 0.12$	$0.02 \pm 0.02$	$0.12 \pm 0.10$	$0.11 \pm 0.19$
	QTRAN [22]	$0.21 \pm 0.08$	$0.27 \pm 0.08$	$0.01 \pm 0.01$	$0.00 \pm 0.00$	$0.00 \pm 0.00$	$0.00 \pm 0.00$
	QPLEX [12]	$0.50 \pm 0.06$	$0.48 \pm 0.09$	$0.05 \pm 0.02$	$0.00 \pm 0.00$	$0.05 \pm 0.09$	$0.01 \pm 0.02$
	OWQMIX [23]	$0.47 \pm 0.10$	$0.41 \pm 0.08$	$0.28 \pm 0.11$	$0.00 \pm 0.00$	$0.29 \pm 0.17$	$0.09 \pm 0.08$
	CWQMIX [23]	$0.49 \pm 0.08$	$0.36 \pm 0.09$	$0.24 \pm 0.11$	$0.00 \pm 0.00$	$0.23 \pm 0.17$	$0.05 \pm 0.04$
	<b>Ours</b>	<b><math>0.68 \pm 0.04</math></b>	<b><math>0.61 \pm 0.05</math></b>	<b><math>0.54 \pm 0.08</math></b>	<b><math>0.59 \pm 0.05</math></b>	<b><math>0.53 \pm 0.12</math></b>	<b><math>0.38 \pm 0.13</math></b>
Test Win Rate	IQL [53]	$0.26 \pm 0.16$	$0.47 \pm 0.09$	$0.00 \pm 0.00$	$0.08 \pm 0.15$	$0.00 \pm 0.00$	$0.00 \pm 0.00$
	VDN [10]	$0.94 \pm 0.04$	$0.73 \pm 0.05$	$0.20 \pm 0.27$	$0.25 \pm 0.21$	$0.00 \pm 0.00$	$0.27 \pm 0.19$
	QMIX [11]	$0.88 \pm 0.13$	$0.57 \pm 0.19$	$0.54 \pm 0.30$	$0.20 \pm 0.18$	$0.37 \pm 0.31$	$0.25 \pm 0.34$
	QTRAN [22]	$0.60 \pm 0.23$	$0.50 \pm 0.20$	$0.02 \pm 0.02$	$0.00 \pm 0.00$	$0.00 \pm 0.00$	$0.00 \pm 0.00$
	QPLEX [12]	$0.79 \pm 0.08$	$0.70 \pm 0.09$	$0.44 \pm 0.14$	$0.01 \pm 0.01$	$0.13 \pm 0.27$	$0.08 \pm 0.14$
	OWQMIX [23]	$0.75 \pm 0.14$	$0.54 \pm 0.18$	$0.62 \pm 0.27$	$0.00 \pm 0.00$	$0.54 \pm 0.27$	$0.34 \pm 0.23$
	CWQMIX [23]	$0.77 \pm 0.12$	$0.56 \pm 0.11$	$0.69 \pm 0.19$	$0.00 \pm 0.00$	$0.35 \pm 0.29$	$0.16 \pm 0.13$
	<b>Ours</b>	<b><math>0.97 \pm 0.02</math></b>	<b><math>0.86 \pm 0.07</math></b>	<b><math>0.96 \pm 0.03</math></b>	<b><math>0.88 \pm 0.08</math></b>	<b><math>0.94 \pm 0.03</math></b>	<b><math>0.84 \pm 0.17</math></b>

training. The results suggest that the disentangling can be utilized to explore the diverse cooperation mechanisms, which helps the agents to construct a more useful policy and achieves non-trivial performance.

To further test the potentiality of our proposed method, we compare our method in the super hard heterogeneous scenarios (*MMM2*, *corridor*, *6h\_vs\_8z*, *3s5z\_vs\_3s6z*). In these challenging scenarios, extracting interaction patterns becomes complex due to the different unit types. Furthermore, there is a great disparity in strength between the two teams, and it is impossible to beat the enemies in a reckless way. The agents have to learn proper tactics to win the battle, while the sophisticated tactics are laborious to explore. In the *MMM2* and *6h\_vs\_8z* scenarios, *OWQMIX* and *CWQMIX* use a weighted projection that allows more emphasis to be placed on better joint actions, giving their improved ability in cooperative exploration. Even so, they inevitably fall into suboptimal policies with low test win rates. In contrast, the proposed OPT provides an impressive improvement in the performance over the baselines, showing its robustness to an increased rate and quality of exploration. Especially in the *corridor* and *3s5z\_vs\_3s6z* scenarios, almost all compared baselines cannot learn any effective policy and perform poorly. Our method still maintains a high learning efficiency, and in practice, leads to the superior performance compared to the baselines.

## 5.2 Multi-task Environment

To further evaluate the proposed method in a multi-task setting, we conduct experiments on 6 multi-task SMAC

scenarios, including 3 basic scenarios (*3-8csz*, *3-8MMM*, *3-8sz*) proposed by *REFIL* [13] and 3 new harder scenarios (*5-11csz*, *5-11MMM*, *5-11sz*). The *3-8sz* scenarios contains 39 unique tasks of different scales, and the *3-8MMM* and *3-8csz* scenarios contain 66 tasks respectively. We follow the multi-task setting of *REFIL* [13] and design 3 new harder scenarios: (1) *5-11csz* contains two symmetrical teams, each of which is composed of 5 to 8 *Stalkers/Zealots* and 0 to 3 *Colossi*, resulting in 120 unique tasks. (2) *5-11sz* contains two symmetrical teams, each of which is composed of 5 to 11 *Stalkers/Zealots*, resulting in 63 unique tasks. (3) *5-11MMM* contains two symmetrical teams, each of which is composed of 5 to 8 *Marines/Marauders* and 0 to 3 *Medics*, resulting in 120 unique tasks. According to the difficulty of training, we can also divide these scenarios into three categories: **Easy** (*3-8csz*, *5-11csz*), **Hard** (*3-8MMM*, *3-8sz*) and **Super Hard** (*5-11MMM*, *5-11sz*). We compare the proposed OPT with various multi-task baselines: *VDN* [10], *QMIX* [11], *REFIL* [13]. We realize the attention-based *VDN* and *QMIX* for the multi-task setting as in *REFIL* [13]. The models train simultaneously on multiple tasks sampled uniformly at each episode. For more exploration, we extend the epsilon anneal time to 500K for all the compared methods.

The proposed method is particularly beneficial in this multi-task setting, which enables us to explore the diverse common interaction prototypes and generalize across various-scale tasks. Figure 5 and Table 2 report the experimental results of all comparison methods on 6 multi-task scenarios. The results show that our proposed method consistently outperforms the baselines, which demonstrate the effectiveness of interaction pattern disentangling. In the

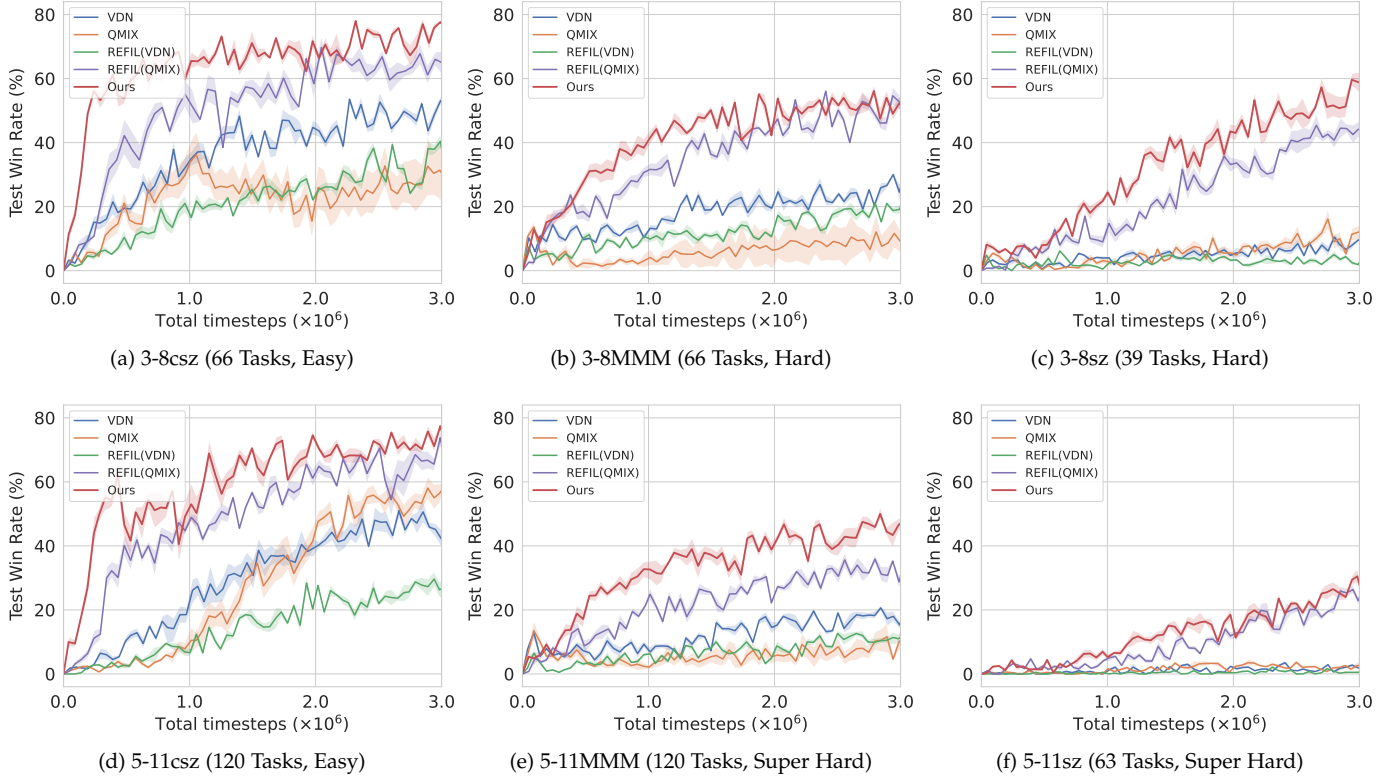
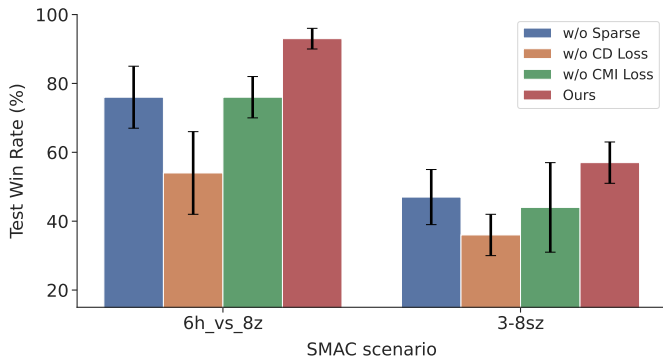


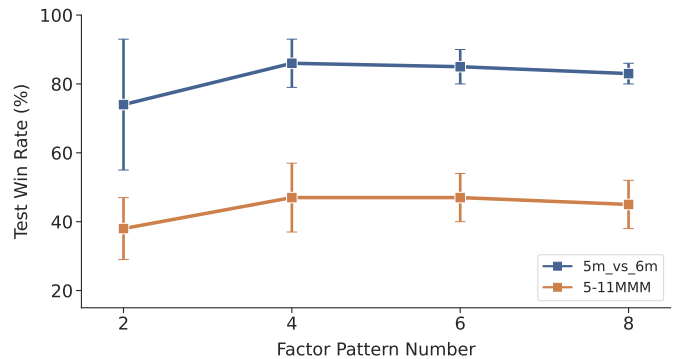
Fig. 5: Learning curves of our method and baselines in 6 multi-task SMAC scenarios.

TABLE 2: The area under curve and test win rate of our method and baselines in 6 multi-task SMAC scenarios.

	Method	3-8sz	3-8MMM	3-8csz	5-11sz	5-11MMM	5-11csz
Area Under Curve	VDN [10]	0.05 $\pm$ 0.01	0.18 $\pm$ 0.02	0.36 $\pm$ 0.03	0.01 $\pm$ 0.00	0.12 $\pm$ 0.01	0.29 $\pm$ 0.05
	QMIX [11]	0.05 $\pm$ 0.02	0.06 $\pm$ 0.08	0.22 $\pm$ 0.13	0.02 $\pm$ 0.00	0.06 $\pm$ 0.05	0.27 $\pm$ 0.06
	REFIL(VDN) [13]	0.03 $\pm$ 0.01	0.12 $\pm$ 0.01	0.21 $\pm$ 0.03	0.00 $\pm$ 0.00	0.07 $\pm$ 0.01	0.14 $\pm$ 0.01
	REFIL(QMIX) [13]	0.23 $\pm$ 0.02	0.35 $\pm$ 0.01	0.51 $\pm$ 0.05	0.10 $\pm$ 0.01	0.22 $\pm$ 0.01	0.48 $\pm$ 0.02
Ours		<b>0.32 <math>\pm</math> 0.03</b>	<b>0.40 <math>\pm</math> 0.03</b>	<b>0.65 <math>\pm</math> 0.02</b>	<b>0.13 <math>\pm</math> 0.02</b>	<b>0.33 <math>\pm</math> 0.02</b>	<b>0.60 <math>\pm</math> 0.03</b>
Test Win Rate	VDN [10]	0.06 $\pm$ 0.02	0.24 $\pm$ 0.04	0.52 $\pm$ 0.10	0.01 $\pm$ 0.01	0.15 $\pm$ 0.02	0.42 $\pm$ 0.10
	QMIX [11]	0.11 $\pm$ 0.07	0.08 $\pm$ 0.10	0.28 $\pm$ 0.27	0.01 $\pm$ 0.01	0.11 $\pm$ 0.09	0.56 $\pm$ 0.12
	REFIL(VDN) [13]	0.06 $\pm$ 0.03	0.20 $\pm$ 0.04	0.39 $\pm$ 0.06	0.00 $\pm$ 0.00	0.12 $\pm$ 0.05	0.29 $\pm$ 0.08
	REFIL(QMIX) [13]	0.44 $\pm$ 0.07	0.53 $\pm$ 0.07	0.66 $\pm$ 0.12	0.25 $\pm$ 0.05	0.27 $\pm$ 0.01	0.65 $\pm$ 0.08
	Ours	<b>0.57 <math>\pm</math> 0.06</b>	<b>0.53 <math>\pm</math> 0.03</b>	<b>0.79 <math>\pm</math> 0.06</b>	<b>0.27 <math>\pm</math> 0.03</b>	<b>0.47 <math>\pm</math> 0.10</b>	<b>0.75 <math>\pm</math> 0.07</b>



(a) Ablation study on three major components.



(b) Ablation study on the interaction prototype number.

Fig. 6: Comparing results over the ablations of OPT.

easy scenarios (3-8csz, 5-11csz), REFIL can also learn effective cooperation strategies based on its random grouping mechanism. However, the latent interaction patterns still remain entangled in REFIL, which may severely downgrade the convergence rate. Conversely, our proposed OPT allows for the explicit shareable pattern disentangling across tasks, improving the learning efficiency and performance of the agents. In the hard 3-8MMM scenario, OPT achieves the performances on par with REFIL and still maintains a higher learning efficiency. Moreover, in the more difficult 3-8sz and 5-11MMM scenario, OPT demonstrates its advantages in the transferability of the common prototypes and achieves gratifying results. In the super hard 5-11sz scenario, the performance gap between OPT and REFIL is not obvious, but most baselines including Attn (VDN), Attn (QMIX), REFIL (VDN) fail to learn any effective policy. To this end, OPT also successfully discovers several effective common interaction prototypes.

### 5.3 Ablations and Visualization

To understand the superior performance of OPT, we carry out ablation studies to test the contribution of its three main components: sparsemax, contrastive disagreement (CD) loss and conditional mutual information (CMI) loss. Following methods are included in the evaluation: (i) OPT without sparsemax (denoted by *w/o Sparse*); (ii) OPT without CD loss (denoted by *w/o CD Loss*); (iii) OPT without CMI loss

(denoted by *w/o CMI Loss*). The results on both the single-task and multi-task scenarios are shown in Figure 6a. By comparing OPT without sparsemax and without CD loss, we can conclude that sparsity can help facilitate learning but the significant performance of OPT is mostly due to the restriction of CD loss. CD loss constrains the interaction prototypes to uniformly distribute on a hypersphere without divergence, which makes a major contribution to interaction pattern disentangling. Sparsemax mainly serves as an auxiliary means that constructs the more compact interaction prototypes. Moreover, CMI loss aims to stabilize the training process. When without CMI loss, the optimization results often derive a high standard deviation, especially in the multi-task scenario. This instability also leads to a significant drop in the performance.

Moreover, to study the impact of the interaction prototype number on the performance of OPT, we conduct an ablation study as shown in Figure 6b. When the number of interaction prototypes increases from 2 to 4, the performance gain of OPT becomes larger. This result verifies the effectiveness of the interaction pattern disentangling. Different interaction prototypes still remain entangled when the number of interaction prototypes is small, resulting in a worse performance. However, as the number of interaction prototypes becomes too large, disentanglement will be more challenging, yielding lower performance gains. After reaching the peak at 4, the performance slightly drops, but in

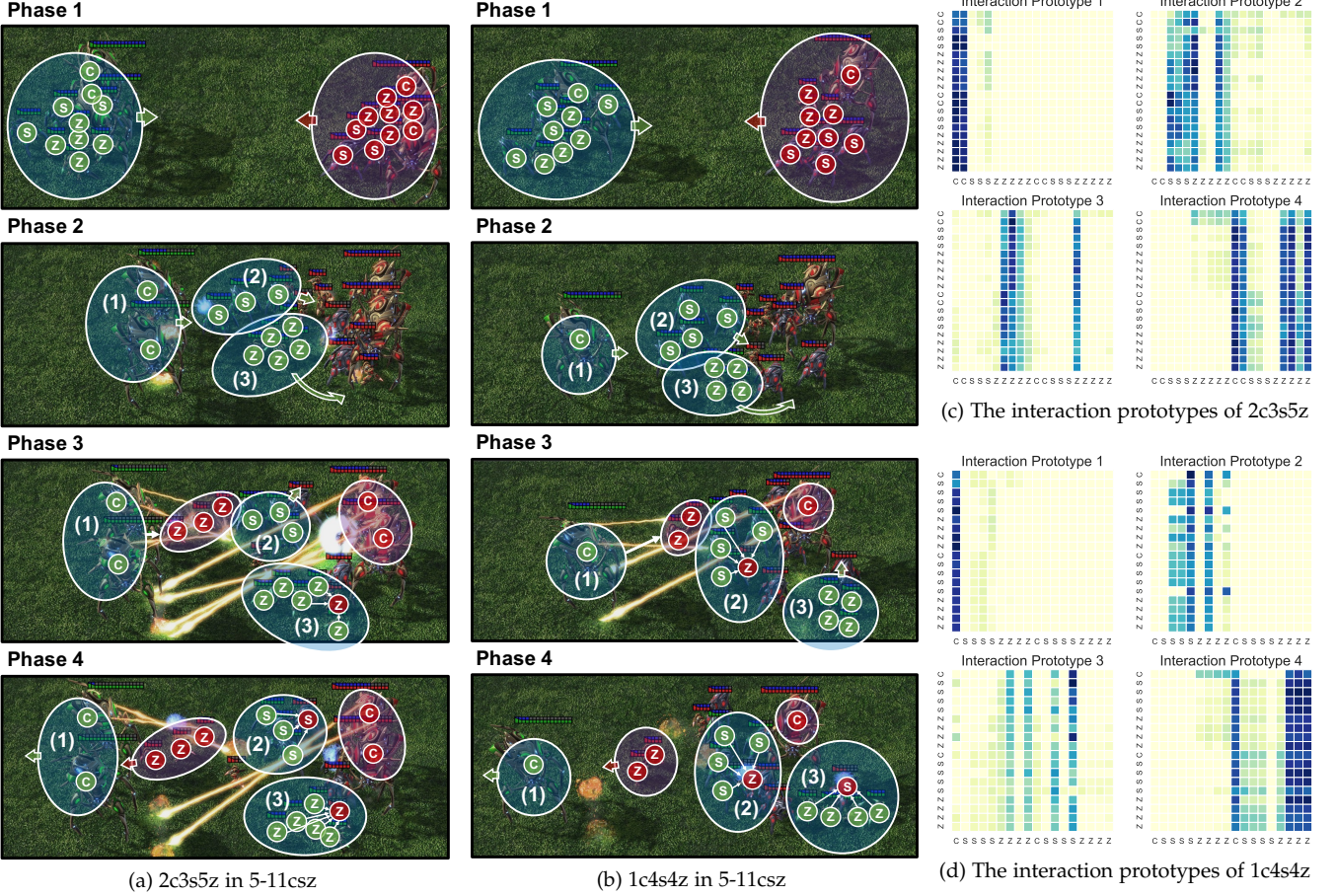


Fig. 7: A visualization example of the common interaction prototypes that emerge across tasks in the 5-11csz scenario. Please zoom for better view. (a) Each combat team of 2c3s5z is composed of 2 Colossi, 3 Stalkers and 5 Zealots. (b) Each combat team of 1c4s4z is composed of 1 Colossus, 4 Stalkers and 4 Zealots. Green and red shadows indicate the agent and enemy formations, respectively. Green and red arrows indicate the moving direction of the agent and enemy formations, respectively. White arrows indicate the attack action of the agents. (c) The interaction prototypes of 2c3s5z in the mixing network at phase 4. (d) The interaction prototypes of 1c4s4z in the mixing network at phase 4. The entities on the axes are arrayed by agents first and enemies later. Diverse common tactics based on the common prototypes emerge in combat tasks with different scales: (1) Hit and Run based on Prototype 1&4, i.e., drawing the fire, moving the agents away and fighting back again. (2) Coordinated Move and Force Fire based on Prototype 2, i.e., moving together and focusing fire on an enemy. (3) Sneak Attack based on Prototype 3, i.e., sneaking around behind the enemy and attacking the alone enemy.

general, our method is not very sensitive when the number of interaction prototypes is large. More interestingly, we find that the standard deviation of the results becomes smaller as the number of interaction prototypes increases, which indicates that providing more interaction prototypes for restructuring enables the agents to stabilize the final policy.

To further explain the learned interaction prototypes from OPT, we conduct a qualitative analysis. As shown in Figure 7a and 7b, we find that OPT can effectively grasp diverse tactics and utilize these common tactics across various-scale tasks. At the beginning of the battle, two combat teams first get closer to each other. Then our combat team assembles the agents into formations based on their unit types. Since Colossus is a heavy support unit with high defense and a large shooting range, Colossi learn to draw the fire by kiting the enemies. Colossi make the enemies give chase while maintaining enough distance, so that little or no damage is incurred. Moreover, Stalkers often tend to

move together and focus fire on an enemy due to their high attack damage. Most interestingly, Zealots master the ability of sneak attack, which bypasses the disadvantages of low defense and low attack damage. The visualization of the interaction prototypes in Figure 7c and 7d shows that our proposed method successfully disentangles the interaction pattern into several interaction prototypes that are sparse and distinguishable. Moreover, the interaction prototypes between different tasks are highly similar, which verifies the generalization of these prototypes. The shareable interaction prototypes enable our agents to construct and reuse the effective policy, and finally improve the performance of the model.

## 6 CONCLUSION

In this work, we propose a novel approach, termed as OPT, that enables us to take advantage of the factorized

interaction prototypes for multi-agent reinforcement learning. OPT follows a restructuring-by-disentangling scheme, where several distinguishable sparse prototypes are generated and then selectively reassembled together for the final focused policy. We validate OPT over several StarCraft II micromanagement benchmarks, and showcase that it yields results significantly superior to the state-of-the-art techniques in both single-task and multi-task settings. To our best knowledge, this paper is the first attempt towards interaction pattern disentangling in MARL. In our future work, we will extend our method to design a more lightweight disentanglement framework for the large-scale problem, which is more challenging in terms of the exponential complexity as the number of agents increases.

## APPENDIX

### PROOF OF THE CMI LOSS

We propose a conditional mutual information (CMI) objective in the utility network to stabilize the aggregation weights:

$$I(\omega_t^a; \tau_{t-1}^a | o_t^a).$$

Based on the variational inference, we introduce a variational approximator  $q_\psi$  parameterised by  $\psi$  to approximate the posterior  $p(\omega_t^a | \tau_{t-1}^a, o_t^a)$  and derive a tractable lower bound of the CMI objective:

$$\begin{aligned} & I(\omega_t^a; \tau_{t-1}^a | o_t^a) \\ &= H(\omega_t^a | o_t^a) - H(\omega_t^a | \tau_{t-1}^a, o_t^a) \\ &= H(\omega_t^a | o_t^a) + \mathbb{E}_{\tau_{t-1}^a, o_t^a} \left[ \mathbb{E}_{\omega_t^a} [\log p(\omega_t^a | \tau_{t-1}^a, o_t^a)] \right] \\ &= H(\omega_t^a | o_t^a) + \mathbb{E}_{\tau_{t-1}^a, o_t^a} \left[ \mathbb{E}_{\omega_t^a} [\log p(\omega_t^a | \tau_{t-1}^a, o_t^a) \right. \\ &\quad \left. - \log q_\psi(\omega_t^a | \tau_{t-1}^a, o_t^a) + \log q_\psi(\omega_t^a | \tau_{t-1}^a, o_t^a)] \right] \\ &= H(\omega_t^a | o_t^a) + \mathbb{E}_{\tau_{t-1}^a, o_t^a} \left[ \mathbb{E}_{\omega_t^a} [\log q_\psi(\omega_t^a | \tau_{t-1}^a, o_t^a)] \right] \\ &\quad + \mathbb{E}_{\tau_{t-1}^a, o_t^a} \left[ \text{KL}[p(\omega_t^a | \tau_{t-1}^a, o_t^a) \| q_\psi(\omega_t^a | \tau_{t-1}^a, o_t^a)] \right]. \end{aligned}$$

Due to the non-negativity of the KL divergence, we can obtain the lower bound of the CMI objective as

$$\begin{aligned} & I(\omega_t^a; \tau_{t-1}^a | o_t^a) \\ &\geq H(\omega_t^a | o_t^a) + \mathbb{E}_{\tau_{t-1}^a, o_t^a} \left[ \mathbb{E}_{\omega_t^a} [\log q_\psi(\omega_t^a | \tau_{t-1}^a, o_t^a)] \right]. \end{aligned}$$

Then we further simplify this lower bound as follows:

$$\begin{aligned} & H(\omega_t^a | o_t^a) + \mathbb{E}_{\tau_{t-1}^a, o_t^a} \left[ \mathbb{E}_{\omega_t^a} [\log q_\psi(\omega_t^a | \tau_{t-1}^a, o_t^a)] \right] \\ &= H(\omega_t^a | o_t^a) + \mathbb{E}_{\tau_{t-1}^a, o_t^a} \left[ \int p(\omega_t^a | o_t^a) \log q_\psi(\omega_t^a | \tau_{t-1}^a, o_t^a) \right] \\ &= H(\omega_t^a | o_t^a) - \mathbb{E}_{\tau_{t-1}^a, o_t^a} \left[ H(p(\omega_t^a | o_t^a), q_\psi(\omega_t^a | \tau_{t-1}^a, o_t^a)) \right] \\ &= - \mathbb{E}_{\tau_{t-1}^a, o_t^a} \left[ \text{KL}[p(\omega_t^a | o_t^a) \| q_\psi(\omega_t^a | \tau_{t-1}^a, o_t^a)] \right]. \end{aligned}$$

Therefore, our final CMI objective can be formalized as a loss function:

$$\mathcal{L}_{CMI}(\theta, \phi, \psi) = \mathbb{E}_{\mathcal{D}} \left[ \text{KL}[p_\phi(\omega_t^a | \bar{x}_t^a) \| q_\psi(\omega_t^a | h_{t-1}^a, \bar{x}_t^a)] \right],$$

where  $\text{KL}(\cdot)$  is the KL divergence function,  $\bar{x}_t^a$  is the input embedding of the observation  $o_t^a$  after mean pooling operation, and a GRU network is used to encode the history trajectory  $\tau_{t-1}^a$  into  $h_{t-1}^a$ .

## REFERENCES

- [1] R. S. Sutton and A. G. Barto, *Reinforcement learning: An introduction*. MIT press, 2018.
- [2] V. Mnih, K. Kavukcuoglu, D. Silver, A. A. Rusu *et al.*, "Human-level control through deep reinforcement learning," *Nature*, vol. 518, no. 7540, pp. 529–533, 2015.
- [3] D. Silver, A. Huang, C. J. Maddison, A. Guez *et al.*, "Mastering the game of go with deep neural networks and tree search," *Nature*, vol. 529, no. 7587, pp. 484–489, 2016.
- [4] O. Vinyals, I. Babuschkin, W. M. Czarnecki, M. Mathieu *et al.*, "Grandmaster level in starcraft ii using multi-agent reinforcement learning," *Nature*, vol. 575, no. 7782, pp. 350–354, 2019.
- [5] M. Jaderberg, W. M. Czarnecki, I. Dunning, L. Marris *et al.*, "Human-level performance in 3d multiplayer games with population-based reinforcement learning," *Science*, vol. 364, no. 6443, pp. 859–865, 2019.
- [6] T. Wu, P. Zhou, K. Liu, Y. Yuan, X. Wang, H. Huang, and D. O. Wu, "Multi-agent deep reinforcement learning for urban traffic light control in vehicular networks," *IEEE Transactions on Vehicular Technology*, vol. 69, no. 8, pp. 8243–8256, 2020.
- [7] Z. Yan and Y. Xu, "A multi-agent deep reinforcement learning method for cooperative load frequency control of a multi-area power system," *IEEE Transactions on Power Systems*, vol. 35, no. 6, pp. 4599–4608, 2020.
- [8] X. Xu, Y. Jia, Y. Xu, Z. Xu, S. Chai, and C. S. Lai, "A multi-agent reinforcement learning-based data-driven method for home energy management," *IEEE Transactions on Smart Grid*, vol. 11, no. 4, pp. 3201–3211, 2020.
- [9] J. Wang, W. Xu, Y. Gu, W. Song, and T. Green, "Multi-agent reinforcement learning for active voltage control on power distribution networks," in *Annual Conference on Neural Information Processing Systems*, 2021.
- [10] P. Sunehag, G. Lever, A. Gruslys, W. M. Czarnecki *et al.*, "Value-decomposition networks for cooperative multi-agent learning based on team reward," in *International Joint Conference on Autonomous Agents and Multi- agent Systems*, 2018.
- [11] T. Rashid, M. Samvelyan, C. S. de Witt, G. Farquhar, J. N. Foerster, and S. Whiteson, "QMIX: monotonic value function factorisation for deep multi-agent reinforcement learning," in *International Conference on Machine Learning*, 2018.
- [12] J. Wang, Z. Ren, T. Liu, Y. Yu, and C. Zhang, "QPLEX: duplex dueling multi-agent q-learning," in *International Conference on Learning Representations*, 2021.
- [13] S. Iqbal, C. A. S. de Witt, B. Peng, W. Boehmer, S. Whiteson, and F. Sha, "Randomized entity-wise factorization for multi-agent reinforcement learning," in *International Conference on Machine Learning*, 2021.
- [14] S. Iqbal and F. Sha, "Actor-attention-critic for multi-agent reinforcement learning," in *International Conference on Machine Learning*, 2019.
- [15] J. Jiang and Z. Lu, "Learning attentional communication for multi-agent cooperation," in *Annual Conference on Neural Information Processing Systems*, 2018.
- [16] R. Lowe, Y. Wu, A. Tamar, J. Harb, P. Abbeel, and I. Mordatch, "Multi-agent actor-critic for mixed cooperative-competitive environments," in *Annual Conference on Neural Information Processing Systems*, 2017.
- [17] J. N. Foerster, G. Farquhar, T. Afouras, N. Nardelli, and S. Whiteson, "Counterfactual multi-agent policy gradients," in *AAAI Conference on Artificial Intelligence*, 2018.
- [18] Y. Yang, R. Luo, M. Li, M. Zhou, W. Zhang, and J. Wang, "Mean field multi-agent reinforcement learning," in *International Conference on Machine Learning*, 2018.
- [19] C. Yu, A. Veliu, E. Vinitksy, Y. Wang, A. Bayen, and Y. Wu, "The surprising effectiveness of ppo in cooperative, multi-agent games," *arXiv preprint arXiv:2103.01955*, 2021.
- [20] M. Zhou, Z. Liu, P. Sui, Y. Li, and Y. Y. Chung, "Learning implicit credit assignment for cooperative multi-agent reinforcement learning," in *Annual Conference on Neural Information Processing Systems*, 2020.
- [21] B. Peng, T. Rashid, C. S. de Witt, P. Kamienny, P. H. S. Torr, W. Boehmer, and S. Whiteson, "FACMAC: factored multi-agent centralised policy gradients," in *Annual Conference on Neural Information Processing Systems*, 2021.
- [22] K. Son, D. Kim, W. J. Kang, D. Hostallero, and Y. Yi, "QTRAN: learning to factorize with transformation for cooperative multi-

agent reinforcement learning," in *International Conference on Machine Learning*, 2019.

[23] T. Rashid, G. Farquhar, B. Peng, and S. Whiteson, "Weighted QMIX: expanding monotonic value function factorisation for deep multi-agent reinforcement learning," in *Annual Conference on Neural Information Processing Systems*, 2020.

[24] T. Wang, H. Dong, V. R. Lesser, and C. Zhang, "ROMA: multi-agent reinforcement learning with emergent roles," in *International Conference on Machine Learning*, 2020.

[25] T. Wang, T. Gupta, A. Mahajan, B. Peng, S. Whiteson, and C. Zhang, "RODE: learning roles to decompose multi-agent tasks," in *International Conference on Learning Representations*, 2021.

[26] Q. Long, Z. Zhou, A. Gupta, F. Fang, Y. Wu, and X. Wang, "Evolutionary population curriculum for scaling multi-agent reinforcement learning," in *International Conference on Learning Representations*, 2020.

[27] W. Wang, T. Yang, Y. Liu, J. Hao, X. Hao, Y. Hu, Y. Chen, C. Fan, and Y. Gao, "From few to more: Large-scale dynamic multiagent curriculum learning," in *AAAI Conference on Artificial Intelligence*, 2020.

[28] Q. Fu, T. Qiu, J. Yi, Z. Pu, and S. Wu, "Concentration network for reinforcement learning of large-scale multi-agent systems," in *AAAI Conference on Artificial Intelligence*, 2022.

[29] A. Mahajan, T. Rashid, M. Samvelyan, and S. Whiteson, "MAVEN: multi-agent variational exploration," in *Annual Conference on Neural Information Processing Systems*, 2019.

[30] T. Wang, J. Wang, Y. Wu, and C. Zhang, "Influence-based multi-agent exploration," in *International Conference on Learning Representations*, 2020.

[31] J. Jiang and Z. Lu, "The emergence of individuality," in *International Conference on Machine Learning*, 2021.

[32] C. Li, T. Wang, C. Wu, Q. Zhao, J. Yang, and C. Zhang, "Celebrating diversity in shared multi-agent reinforcement learning," in *Annual Conference on Neural Information Processing Systems*, 2021.

[33] L. Zheng, J. Chen, J. Wang, J. He, Y. Hu, Y. Chen, C. Fan, Y. Gao, and C. Zhang, "Episodic multi-agent reinforcement learning with curiosity-driven exploration," in *Annual Conference on Neural Information Processing Systems*, 2021.

[34] J. Jiang, C. Dun, T. Huang, and Z. Lu, "Graph convolutional reinforcement learning," in *International Conference on Learning Representations*, 2020.

[35] H. Mao, W. Liu, J. Hao, J. Luo, D. Li, Z. Zhang, J. Wang, and Z. Xiao, "Neighborhood cognition consistent multi-agent reinforcement learning," in *AAAI Conference on Artificial Intelligence*, 2020.

[36] H. Ryu, H. Shin, and J. Park, "Multi-agent actor-critic with hierarchical graph attention network," in *AAAI Conference on Artificial Intelligence*, 2020.

[37] S. Hu, F. Zhu, X. Chang, and X. Liang, "Updet: Universal multi-agent RL via policy decoupling with transformers," in *International Conference on Learning Representations*, 2021.

[38] T. Zhou, F. Zhang, K. Shao, K. Li *et al.*, "Cooperative multi-agent transfer learning with level-adaptive credit assignment," *arXiv preprint arXiv:2106.00517*, 2021.

[39] Y. Zhang, Q. Yang, D. An, and C. Zhang, "Coordination between individual agents in multi-agent reinforcement learning," in *AAAI Conference on Artificial Intelligence*, 2021.

[40] T. Wang, L. Zeng, W. Dong, Q. Yang, Y. Yu, and C. Zhang, "Context-aware sparse deep coordination graphs," in *International Conference on Learning Representations*, 2022.

[41] Y. Liu, W. Wang, Y. Hu, J. Hao, X. Chen, and Y. Gao, "Multi-agent game abstraction via graph attention neural network," in *AAAI Conference on Artificial Intelligence*, 2020.

[42] S. Luo, Y. Li, J. Li, K. Kuang, F. Liu, Y. Shao, and C. Wu, "S2rl: Do we really need to perceive all states in deep multi-agent reinforcement learning?" *arXiv preprint arXiv:2206.11054*, 2022.

[43] F. A. Oliehoek and C. Amato, *A Concise Introduction to Decentralized POMDPs*. Springer, 2016.

[44] L. Pan, T. Rashid, B. Peng, L. Huang, and S. Whiteson, "Regularized softmax deep multi-agent q-learning," in *Annual Conference on Neural Information Processing Systems*, 2021.

[45] T. Zhang, Y. Li, C. Wang, G. Xie, and Z. Lu, "FOP: factorizing optimal joint policy of maximum-entropy multi-agent reinforcement learning," in *International Conference on Machine Learning*, 2021.

[46] Y. Yang, J. Hao, G. Chen, H. Tang, Y. Chen, Y. Hu, C. Fan, and Z. Wei, "Q-value path decomposition for deep multiagent reinforcement learning," in *International Conference on Machine Learning*, 2020.

[47] W. Wang, T. Yang, Y. Liu, J. Hao, X. Hao, Y. Hu, Y. Chen, C. Fan, and Y. Gao, "Action semantics network: Considering the effects of actions in multiagent systems," in *International Conference on Learning Representations*, 2020.

[48] A. Vaswani, N. Shazeer, N. Parmar, J. Uszkoreit, L. Jones, A. N. Gomez, L. Kaiser, and I. Polosukhin, "Attention is all you need," in *Annual Conference on Neural Information Processing Systems*, 2017.

[49] A. F. T. Martins and R. F. Astudillo, "From softmax to sparsemax: A sparse model of attention and multi-label classification," in *International Conference on Machine Learning*, 2016.

[50] G. M. Correia, V. Niculae, and A. F. T. Martins, "Adaptively sparse transformers," in *Conference on Empirical Methods in Natural Language Processing*, 2019.

[51] T. Wang and P. Isola, "Understanding contrastive representation learning through alignment and uniformity on the hypersphere," in *International Conference on Machine Learning*, 2020.

[52] K. Cho, B. Van Merriënboer, D. Bahdanau, and Y. Bengio, "On the properties of neural machine translation: Encoder-decoder approaches," *arXiv preprint arXiv:1409.1259*, 2014.

[53] M. Samvelyan, T. Rashid, C. S. de Witt, G. Farquhar, N. Nardelli, T. G. J. Rudner, C. Hung, P. H. S. Torr, J. N. Foerster, and S. Whiteson, "The starcraft multi-agent challenge," in *International Joint Conference on Autonomous Agents and Multi- agent Systems*, 2019.